

# A Neural Network Solution to Design Dual Stator Winding Insulation Level Detector for Three Phase Induction Motors

H. SELCUK NOGAY

Electrical Education Department  
Marmara University Technical Education Faculty  
Goztepe Campus, Kadikoy/Istanbul/TURKEY  
[selcuknogay@marmara.edu.tr](mailto:selcuknogay@marmara.edu.tr)

*Abstract:* This paper implements an Artificial Neural Network (ANN) model able to predict the insulation level in a dual-stator winding squirrel-cage three-phase induction motor fed by an inverter. A sinusoidal pulse-width modulation (SPWM) inverter feeding three-phase induction motors were tested up to over load. The results show that the artificial neural network model produces reliable estimates of Insulation level for dual stator winding.

*Key-Words:* - Artificial neural network (ANN); Three-phase induction motor; Insulation level, Dual Stator winding.

## 1 Introduction

Squirrel cage Induction machines are the standard choice in many industrial applications because of their ruggedness and low cost. For this reason, their reliability and durability is important in many industrial processes and can also have an influence on the widely understood human safety. Fortunately, high reliability and durability are one of the main constructive advantages of induction cage machines. Dangerously, the high temperatures inside the machine may damage the insulation layers of the stator and rotor winding and lamination, and eventually lead to a motor failure. The higher windings temperature causes faster aging of the insulation system and, consequently, shortens the operational life of a machine. Many resources show that 35%–45% of motor failures are caused by stator insulation breakdown.

The dual-stator winding squirrel-cage induction machine is the most recent innovation in the family of induction machinery. There are broadly two designs, the first type has two stator windings wound for the same pole numbers with similar or dissimilar phase numbers while the second design has two stator windings with dissimilar pole numbers with same or unequal phase numbers. There is also the brushless doubly-fed induction machine having two stator windings wound for dissimilar pole numbers and a specially designed nested loop rotor structure which couples the two air-gap flux linkages derived from the two stator windings. Synchronous mode of operation of this the machine appears to be the most profitable especially for converter-based drive control. While the brushless doubly-fed induction machine requires an intricate but expensive nested rotor design, the dual stator winding squirrel-cage induction machine addressed in this paper uses the standard squirrel cage rotor design. Some

unique characteristics and advantages of dual-stator winding induction machines of various types suggest their possible attractiveness in some motoring and generating applications. While the dual stator winding induction machine wound with similar pole numbers have received some intensive research attention, relative little has been done to explore and gain deeper insights into the operability and control of the dual-stator squirrel-cage induction machines.

The dual-stator winding squirrel-cage induction machine considered in this paper consists of a stator with two separate windings, having dissimilar pole numbers, P1 and P2 (e.g., 2/6 or 4/12) and a standard squirrel-cage rotor. The attractive advantages of this kind of machine over the competing others are its better controllability in the very low speed range and the flexibility of the output generator characteristics. Since the air-gap flux linkages created by the two stator windings and the induced rotor currents share the same magnetic stator and rotor cores, the main air-gap flux saturation phenomenon is more complicated than that of the normal single stator winding squirrel-cage induction machine. Because of this complexity, a reconsideration of main flux linkage saturation effect is called for in the design of the machine and in the development and practical implementation of speed/torque control algorithms. To avoid deep magnetic saturation in the stator and rotor cores, rotor and stator teeth, magnetic design methodologies have been suggested both for the dual-stator winding and brushless doubly-fed induction machines. How the time-varying, multi-frequency flux linkages erivable from the currents flowing in the stator windings and rotor bars can be appropriately selected for an optimal machine design is yet a challenging question since these flux linkages combine additively in some

regions and subtractively in others engendering non-uniform main flux magnetic saturation[32].

In this study, a prediction study has been completed to compare the effectiveness of artificial intelligence approach. A two layer feed forward neural network trained by the back propagation technique employed in the dual stator winding insulation level estimation. Therefore, five short chorded, three-phase dual winding induction motors were tested up to over loads and different switching frequencies up to 15 KHz. The number of all measurements results obtained from experiments are 530. 20 % of this data for validation, 20% of this data were used for test and 60 % of this data were used for training the neural network.

## 2 Main Flux Linkage Saturation Effect

Since the two stator windings (ABC and XYZ winding Sets) have dissimilar pole numbers, the mutual inductances between them are zero when the main-flux linkage path is unsaturated while possible coupling may be found in the stator leakage inductances. However, it has been shown in [16] that the couplings between the leakage inductances do not exist such that a dual stator winding induction machine can be treated (on the fundamental frequency basis) as two independent squirrel-cage induction machines coupling through the rotor circuit. The magneto-motive forces (MMFs) resulting in the air-gap flux linkage is the sum of the MMFs due to the currents flowing in the two stator winding sets and the MMFs arising from the induced rotor bar currents. If only the fundamental stator currents and their induced harmonic-rich rotor currents are considered, the airgap flux density therefore has four components given as:

$$\begin{aligned}
 B = & B_{1s} \cos(w_{e1}t - P_1q) + B_{2s} \cos(w_{e2}t - P_2q + a_1) \\
 & + \sum_k B_{1rk} \cos(w_{e1}t + (k - P_1)w_r t - kq + a_{2k}) \quad (1) \\
 & + \sum_k B_{2rk} \cos(w_{e2}t + (k - P_2)w_r t - P_2q + a_{3k})
 \end{aligned}$$

Where,  $B_{s1}$  and  $B_{s2}$  are the peak values of the air gap flux densities contributed by the stator ABC and XYZ winding sets, respectively.  $B_{1rk}$  and  $B_{2rk}$  are the flux densities due to the  $k^{th}$  harmonic MMFs of rotor currents. The dual stator winding squirrel-cage induction machines operate in the asynchronous mode for the development of torque components usually found in the single winding three-phase squirrel-cage induction machine, however additional average torque components can be produced when the absolute values of the slip

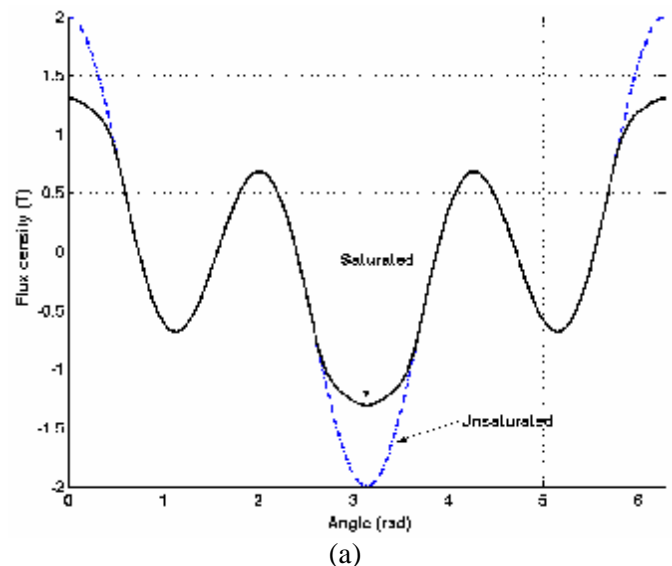
frequencies relative to the two stator windings are equal; i.e

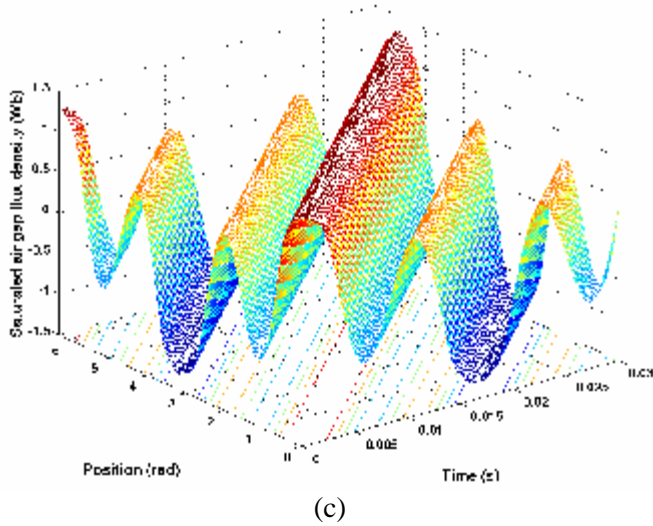
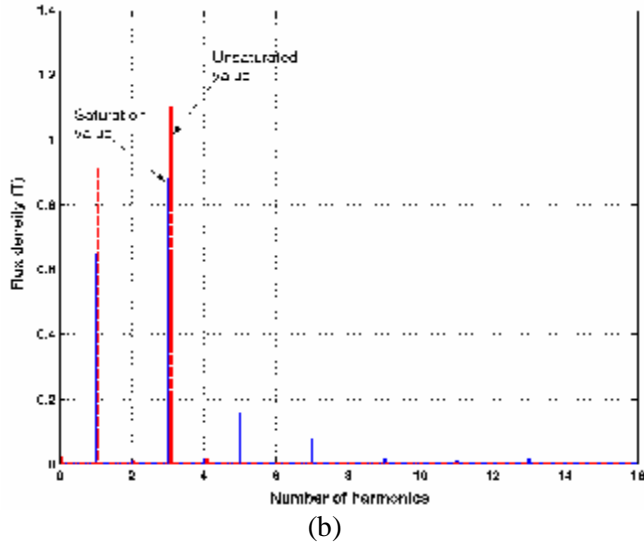
$$w_r = \frac{w_{e1} m w_{e2}}{P_1 m P_2} \quad (2)$$

$$\begin{aligned}
 B = & B_{1s} \cos(w_{e1}t - P_1q) + B_{2s} \cos(w_{e2}t - P_2q + a_1) \\
 & + B_{1rp1} \cos(w_{e1}t - P_1q + a_{2p1}) \quad (3) \\
 & + B_{2rp2} \cos(w_{e2}t - P_2q + a_{3p2})
 \end{aligned}$$

When the speed constraint in (2) is implemented in (1), the resulting fundamental air-gap flux density is given in (3), comprising of components of P1 and P2 poles upon which are superimposed some space harmonics.

When the magnetic circuit is saturated, new saturation induced air-gap flux densities are generated which may link one set of windings to the second set. In the case when the pole pair number combination of the two stator windings is 1/3, the 2-pole winding under main air-gap flux saturation produces a third harmonic component which is commensurate with the flux linkage originating from the 6-pole winding set. By virtue of the phase angle difference between the flux densities due to the 2 and 6-pole windings, the generated saturation flux linkage may reduce or enhance the fundamental air-gap flux linkage due to the 6-pole stator winding set. An understanding of the consequence of the main flux saturation on the air-gap flux density given in (3) is obtained by reviewing Figure 1.





### 3 Explaining the Relations

The voltage equations of dual stator winding induction machine can be expressed in the complex form as [1]:

$$V_{qdsi} = r_{si}i_{qdsi} + pL_{qdsi} - j\omega l_{qdsi} \quad (4)$$

$$V_{qdri} = r_{ri}i_{qdri} + pL_{qdri} - j(\omega - \omega_{ri})L_{qdri} = 0 \quad (5)$$

where,  $i = 1, 2$  represents the (classical) parameters and state variables of ABC and XYZ windings respectively;  $\omega$  is the electrical rotating speed of the common reference frame;  $\omega_{ri}$  is the electrical rotor speed. Since it is easier to account for the magnetic saturation of the main flux linkage using flux linkages as state variables, the currents in (4-5) are eliminated. The flux linkage equations given in terms of currents are:

$$\begin{bmatrix} \lambda_{qdsi} \\ \lambda_{qdri} \end{bmatrix} = \begin{bmatrix} L_{si} & L_{mi} \\ L_{mi} & L_{ri} \end{bmatrix} \times \begin{bmatrix} i_{qdsi} \\ i_{qdri} \end{bmatrix} \quad (6)$$

The stator and rotor currents from (6) can be expressed in terms of the flux linkages as:

$$i_{qdsi} = \frac{L_{ri}}{D_i} \lambda_{qdsi} - \frac{L_{mi}}{D_i} \lambda_{qdri} \quad (7)$$

$$i_{qdri} = \frac{L_{si}}{D_i} \lambda_{qdri} - \frac{L_{mi}}{D_i} \lambda_{qdsi}$$

Where  $D_i = L_{si}L_{ri} - L_{mi}^2$ .

Where  $L_s$  is the stator inductance,  $L_r$  is the rotor inductance  $L_m$  is the mutual inductance between stator and rotor with respect to the corresponding rotor position. From the fundamental electromagnetic theory, the flux linkage of winding is a function of number of equivalent turns. The equivalent turns are expressed by a vector  $N_s = [N_{ms} \ N_{as}]^T$  for the stator winding and  $N_r = [N_{mr} \ N_{ar}]^T$  for the rotor winding. The motor parameters, such as winding resistance and inductance, will change due to changing values of equivalent turns. The same motor structure with different values of equivalent turns will yield a different performance. For a squirrel cage induction motor, the rotor is robust, and  $N_r$  is generally assumed to be constant, while  $N_s$  will change value due to deterioration in the stator winding. When  $N_s$  is variable,  $i_s, L_s, L_m$  become function of  $N_s$ . This can be expressed as, [32]

$$i_s = f_1(N_s) \quad (8)$$

The electrical torque of the motor,  $T_e$ , is a function of

Figure 1: Main flux saturation.  $B_1 = 0.9$  T,  $B_3 = 1.1$ T,  $f_1 = 30$  Hz,  $f_2 = 90$  Hz, (a) Unsaturated and saturated air-gap flux density at  $t = 0.0$ , (b) Fourier series of the unsaturated and saturated waveforms, (c) saturated air-gap flux density distribution as functions of time and circumferential angle [16], [32].

Figure 1(a) shows the unsaturated and saturated air-gap flux density (at time  $t = 0$ ) due to the sum of  $B_1 \cos(\omega_e t - P_1 \theta + \alpha)$  and  $B_2 \cos(\omega_e t - P_2 \theta)$  where  $P_1 = 1, P_2 = 3, B_1 = 0.9$ T,  $B_2 = 1.1$  T and  $\alpha = 0$  is a phase shift angle. The 3-dimensional graph of the saturated air-gap flux density is given in Figure 1(c). The graph of the saturated airgap flux density is obtained using the effective nonlinear BH characteristics of the air-gap magnetic flux path. There are 5th and 7th harmonic components shown in Figure 1(b) resulting from the magnetic air-gap saturation effect. The fundamental and third harmonic flux density components reduce from 0.9 T to 0.647 T and 1.1 T to 0.879 T, respectively [32].

motor parameters and given as,

$$T_e = i_s^T \frac{\partial}{\partial q} M i_r \tag{9}$$

Thus,  $T_e$  is a function of  $N_s$ . The equation of motion for the motor can be written as,

$$T_e(N_s) = J \frac{\partial}{\partial t} w + Bw + T_l \tag{10}$$

Where  $w$  is the rotor speed,  $J$  is the inertia of the rotor and connected load,  $B$  is the damping coefficient of the motor, and  $T_l$  is the load torque, which is assumed to be known. From this equation, it is clear that the rotor speed is also a function of  $N_s$  and can be mentioned as,

$$w = f_2(N_s) \tag{11}$$

A decrease in winding equivalent turns will increase stator winding current; thus causing increased heating due to additional  $I^2R$  losses. The increased heating will cause a corresponding temperature rise in the stator, there by decreasing the life expectancy of the stator winding insulation. Stator winding insulation failure will cause additional shorted turns, further increasing temperature, and this leads to increase in the rate of deterioration of the stator winding insulation. From this, the relation exists between the stator equivalent number of turns, stator current and temperature of winding. Thus, the stator equivalent turns  $N_s$  become the function of temperature,  $\tau$ . This can be expressed as,

$$t = f_3(N_s) \tag{12}$$

Under steady state condition the stator main winding equivalent turns  $N_s$  is used to replace  $N_{ms}$ . Thus, for simplicity of notation,  $N$  is used to replace  $N_s$ , where as  $N_{as}$  will be ignored. Let,  $I$  be the rms value of  $i_{ms}$ ,  $w$  be the average speed of rotor and  $t$  be temperature of motor winding. By combining and manipulating, equations (8), (11) and (12) with main winding equivalent turns ( $N$ ), as variable, the steady-state current ( $I$ ), rotor speed ( $\omega$ ), and temperature of winding ( $\tau$ ) can be represented by a set of nonlinear algebraic equations,  $f = [f_1, f_2, f_3]$ , which are functions of main winding equivalent turns,  $N$ . Therefore, the nonlinear equation can be given as,

$$f(I, w, t, N) = 0 \tag{13}$$

This equation suggests that indications of the condition of the winding can be obtained from the measurements of the stator current ( $I$ ), rotor speed ( $\omega$ ), and the stator

winding temperature ( $\tau$ ). These parameters ( $I, w, t$ ) can be measured easily and are found to be very sensitive to the changing conditions of the stator winding. From the induction motor dynamics analysis given in equation (9), there exists a relationship  $\mu_1$  between ( $I, w, t$ ) to  $N$  as shown in (14).

$$m_1 : (I, w, t) \rightarrow (N) \tag{14}$$

For the present application, the values of  $N$ , which quantitatively describes the motor, are quantized into three conditions (good, fair and bad) to yield  $N_c$ , which qualitatively describes the motor condition. This qualitative description of the motor's condition is more suitable for the detection of winding insulation condition. A second relationship  $m_2$  is used to denote the relationship from quantitative description  $N$  to qualitative description  $N_c$  is given below;

$$m_2 : (N) \rightarrow (N_c) \tag{15}$$

As a result, the relationship  $m$  from ( $I, w, t$ ) to  $N_c$  can be written as composition of  $m_1$  and  $m_2$ .

$$m : m_1 * m_2 : (I, w, t) \rightarrow (N_c) \tag{16}$$

Mapping  $m$  is very complex due to high degree of nonlinearity of induction motor dynamics and of discretization involved. Thus obtaining an accurate analytical expression for  $m$  for a given induction motor is rather difficult. However this complexity can be avoided by training a neural network to learn the desired mapping of  $m$  based solely on input-output examples that can be obtained accurately [2].

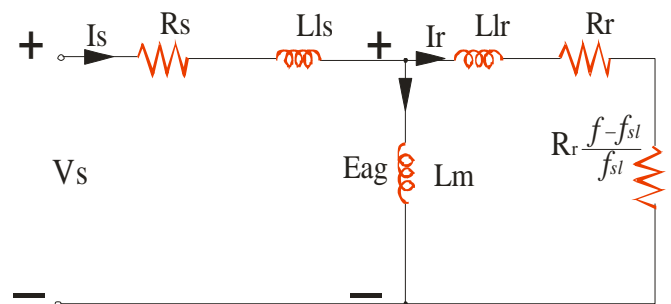


Fig. 2 Equivalent Circuit per Phase for Induction Motors

### 4 Artificial Neural Network (ANN)

There are multitudes of different types of ANN models. Some of the more popular of them include the multilayer perceptron, which is generally trained with the back propagation algorithm. Back propagation is a training

method for multilayer feed forward networks. Such a network including three layers of perceptrons is shown in Figure3 [2].

By the algorithmic approach known as Levenberg-Marquardt back propagation algorithm, the error is decreased repeatedly. Some ANN models employ supervisory training while others are referred to as non-supervisory or self-organizing training. However, the vast majority of ANN models use supervisory training. The training phase may consume a lot of time. In the supervisory training, the actual output of ANN is compared with the desired output. The training set consists of presenting input and output data to the network. The network adjusts the weighting coefficients, which usually begin with random set, so that the next iteration will produce a closer match between the desired and the actual output. The training method tries to minimize the current errors for all processing elements. This global error reduction is created over time by continuously modifying the weighting coefficients until the ANN reaches the user defined performance level. This level signifies that the network has achieved the desired statistical accuracy for a given sequence of inputs. When no further training is necessary, the weighting coefficients are frozen for the application. After a supervisory network performs well on the training data, then it is important to see what it can do with data it has not seen before. If a system does not give reasonable outputs for this test set, the training period is not over. Indeed, this testing is critical to insure that the network has not simply memorized a given set of data, but has learned the general patterns involved within an application [1], [2].

### 3.1 Estimation technique

In order to use the ANN simulator for any application, first the number of neurons in the layers, type of activation function (purelin, tansig, logsig), the number of patterns, and the training rate must be chosen.

### 3.2 Designing of the Model

ANN designing process involves five steps. These are gathering input data, normalizing the data, selecting the ANN architecture, training the network, and testing the network. In the training step, five input variables: Phase current, coil pitches angles, carrier frequency (KHz), interior temperature of the stator winding, rotor speed ( $n$ ) as revolution per minute (rpm) and the output variable: insulation level. The Insulation levels are quantized into three conditions (good, fair and bad) to yield  $N_c$ , which qualitatively describes the motor condition. This qualitative description of the motor's condition is mote suitable for the detection of winding insulation condition.

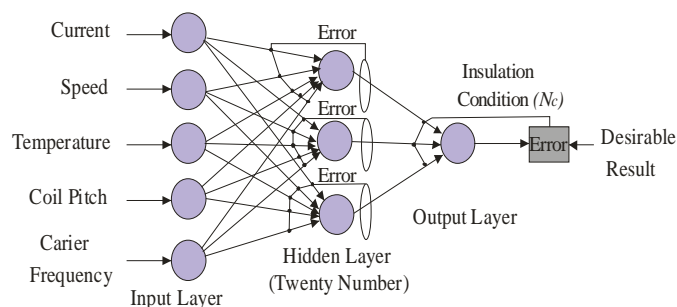


Fig.3 Back propagation of error

### 3.3 Gathering the Data

Experimental set up is shown in Fig. 4. Experimental set up consists of a three-phase PWM inverter which gives output by comparing the modulating signal with carrier signal technique at variable switching frequencies from one to 15 KHz and supplies 50Hz, 380V (r m s) voltage to a three-phase squirrel cage induction motor under test. The operating data of the induction motors are transmitted to the PC through RS-485 for later analysis. Each motor was loaded by an electromagnetic brake which is controlled by the dc voltage applied to the brake provided with two arms, one of which with balances weight for measuring the out put torque of the motor. The brake includes a cooling fan that is supplied by the main voltage. Force applied to the induction motor is measured with a dynamometer which is mounted on the electromagnetic brake's one arm to obtain the applied force. The dual stator winding of five commercial, 1100W, 36-slots, three-phase, four-pole squirrel cage induction motors were loaded with applied torque of from 1 to 9,74 Nm for 1.1 kW and 7.8 Nm for 0.75 kW (full load was 8,18 Nm for 1.1 kW and 6.2 Nm for 0.75 kW). The power and harmonic analyzer employs the fast Fourier transformation to obtain the harmonic voltage components with PWM supply was used [4].

The motors were re-wounded with different coil pitches. The coil pitch for each motor was re-wound to pitch  $180^\circ$  (Full pitch, 1-10 slots pitch),  $160^\circ$  (1-9),  $140^\circ$  (1-8),  $120^\circ$  (1-7) and  $100^\circ$  (1-6) for M1, M2, M3, M4 and M5 motors, respectively. The slot pitch is  $20^\circ$  so for full pitch winding the coil pitch is  $180^\circ$  and the coil pitch is reduced by  $20^\circ$  each time for other motors resulting in coil pitch of  $160^\circ$ ,  $140^\circ$ ,  $120^\circ$  and  $100^\circ$  respectively [4].

Winding configuration of the stators are illustrated in fig. 5. The letters (a, b, and c) indicate the conductors corresponding with phases  $L_1$ ,  $L_2$ ,  $L_3$  and their vertical position designate conductors in the same slot. The direction of current is indicated by a, A etc. The pole pitch is 9 slots with 3 conductor slots per pole per

phase. The slot pitch is  $20^{\circ}$  so for full pitch winding the coil pitch is  $180^{\circ}$  and the coil pitch is reduced by  $20^{\circ}$  each time for other motors resulting in coil pitch of  $160^{\circ}$ ,  $140^{\circ}$ ,  $120^{\circ}$  and  $100^{\circ}$  respectively. To measure the winding temperature, K-type thermocouples were attached to the stator winding of all five motors.

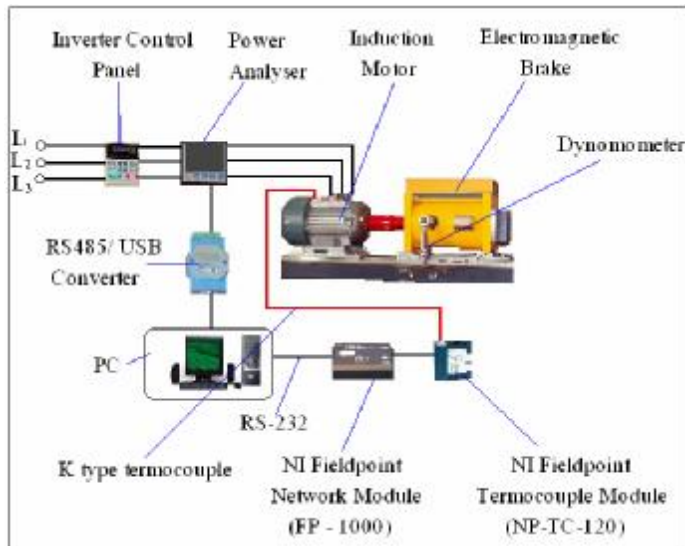


Fig. 4 Experimental setup

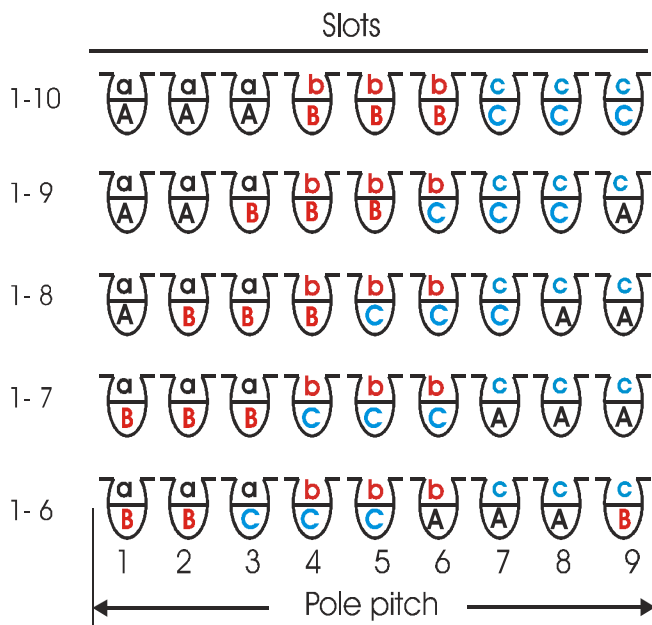


Fig. 5 Three – Phase winding with two layer configuration in the stator slots

### 3.4 Normalization

Normalization of data is a process of scaling the numbers in a data set to improve the accuracy of the subsequent numeric computations and is an important stage for training of the ANN. Normalization also helps in shaping the activation function. For this reason,  $[+1, -1]$  normalization function has been used.

### 3.5 Selecting the ANN Architecture

The number of layers and the number of processing elements per layer are important decisions for selecting the ANN architecture. Choosing these parameters to a feed forward back propagation topology is the art of the ANN designer. There is no quantifiable, best answer to the layout of the network for any particular application. There are only general rules picked up over time and followed by most researchers and engineers applying this architecture to their problems. The first rule states that if the complexity in the relationship between the input data and the desired output increases, then the number of the processing elements in the hidden layer should also increase. The second rule says that if the process being modeled is separable into multiple stages, then additional hidden layer(s) may be required. The result of the tests has showed that the optimal number of neurons in the first layer can be chosen as 20 also, the activation function has been chosen as a hyperbolic tangent sigmoid function for all of the layers [1].

### 3.6 Training the Network

ANN simulator has been trained through the 16 epochs. The training process has been stopped when the error has become stable. Variation of the total absolute error through the epochs is shown in Figure 11.

### 3.6 Testing the Network

In the test, an unknown input pattern has been presented to the ANN, and the output has been calculated. Linear regression between the ANN output and target is performed. After ANN learning and test steps founded regression coefficients ( $R = 0.98081$  and  $R = 0.97711$ ) shows that target and ANN output values were very related each other. These regression analyses were shown in figure 8 and figure 9 respectively for learning step. These coefficient shows that target and ANN output values were very related each other.

### 5 Conclusion

The ANN results are illustrated in Table 1. Variation of the artificial neural network output data together with the target data are illustrated in fig. 6. Variation of the mean square error through the epochs is illustrated in fig. 11. Also on Table 2, 3 and 4, training, validation and test results of ANN model at random twenty five places and at the various data points' indices are illustrated. The results have shown that the prediction error obtained by ANN model is very plausible. So the ANN model produces reliable estimates of insulation level conditions. The results have also pointed out that ANN can implement many other data prediction efforts easily and successfully.

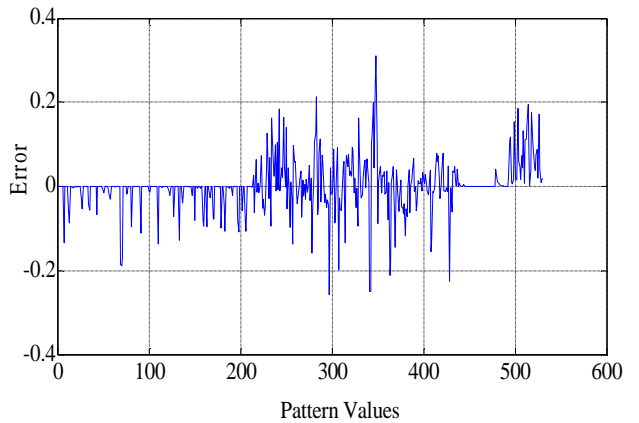


Fig. 7 Variation of the ANN error

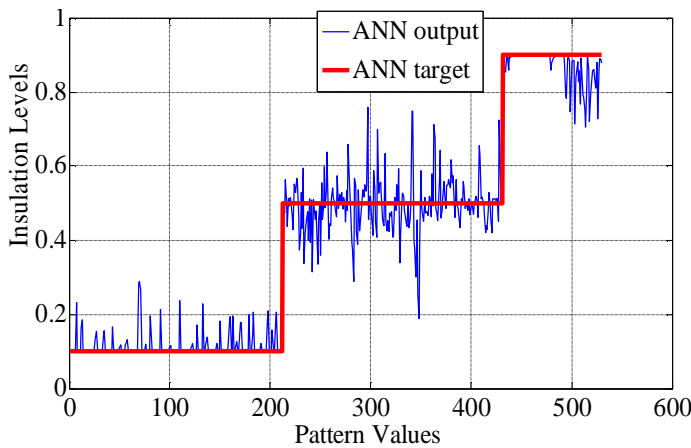


Fig. 6 Variation of the ANN output data together with the target data.

Table 1 ANN results

	Train	Validation	Test
indices	1x318	1x106	1x106
Performance	0.020243	0.031427	0.025108
regression	0.98081	0.97172	0.97715

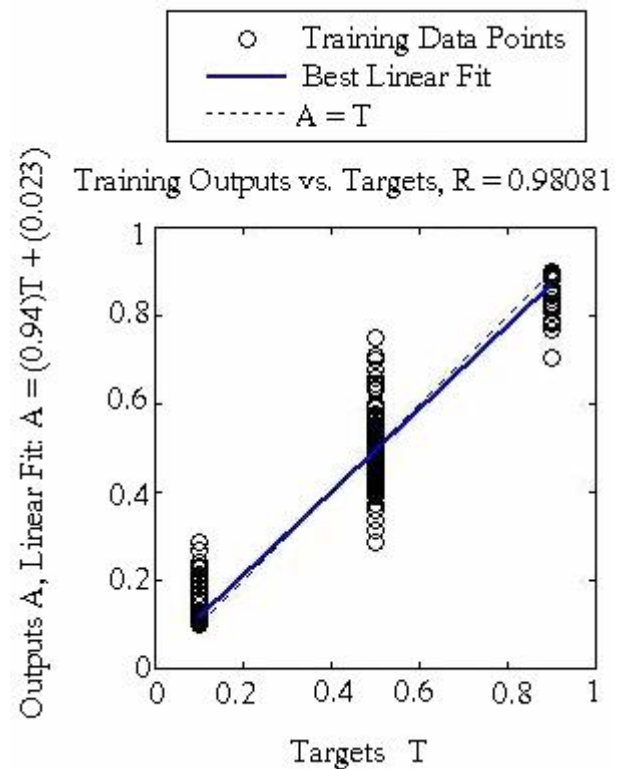


Fig. 8 Linear regression results between the ANN Training results and target

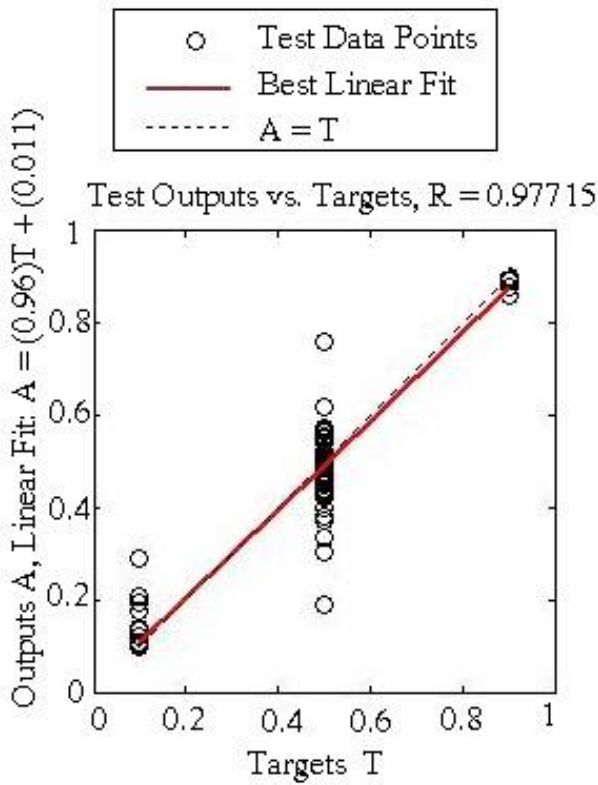


Fig. 9 Linear regression results between the ANN test results and target.

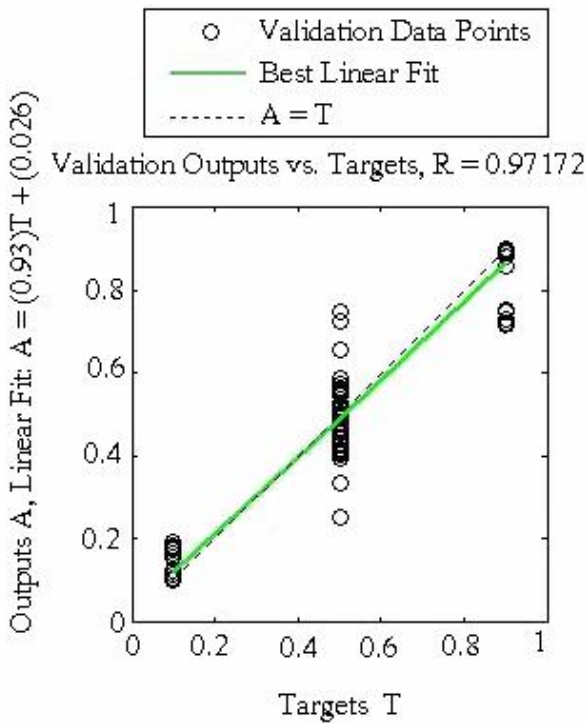


Fig. 10 Linear regression results between the validation data and target.

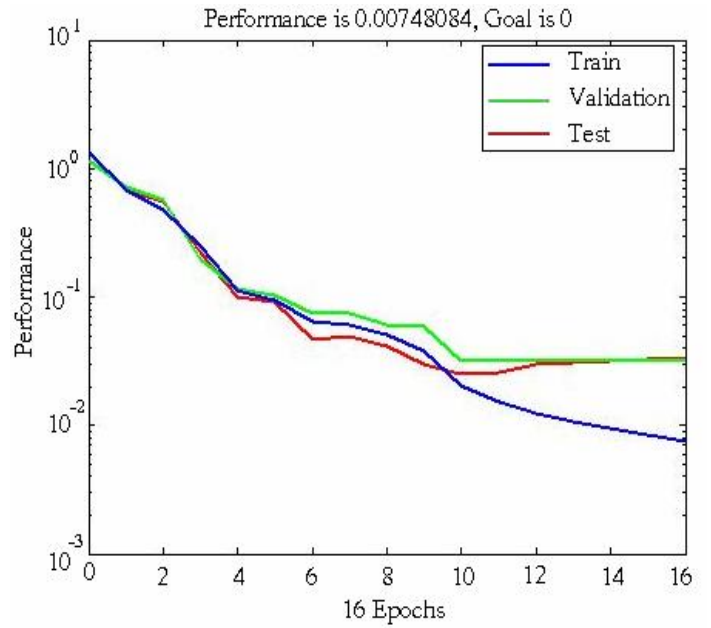


Fig. 11 Variation of the mean square error through the epochs

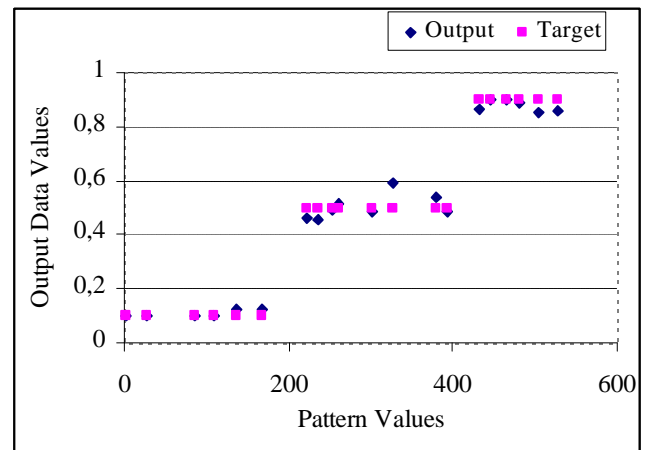


Fig. 12 Variation of the ANN Training results together with the target data for Table 2.

Table 2 Training results at various data points

Indices	Output	Target
2	0.1	0.1
28	0.1	0.1
86	0.1	0.1
109	0.1	0.1
136	0.1234	0.1
167	0.1272	0.1
222	0.4621	0.5
236	0.4549	0.5
253	0.4933	0.5
261	0.5128	0.5
301	0.4828	0.5
328	0.5932	0.5
379	0.5411	0.5
394	0.4872	0.5
432	0.863	0.9
447	0.8999	0.9
465	0.8999	0.9
481	0.8885	0.9
505	0.8534	0.9
527	0.858	0.9

Table 3 Validation results at various data points

Indices	Output	Target
9	0.1	0.1
35	0.156	0.1
51	0.1168	0.1
62	0.1007	0.1
83	0.1	0.1
116	0.1	0.1
121	0.1075	0.1
140	0.1001	0.1
160	0.1936	0.1
200	0.1001	0.1
235	0.419	0.5
310	0.557	0.5
342	0.7483	0.5
371	0.4814	0.5
407	0.4614	0.5
419	0.4969	0.5
462	0.9	0.9
478	0.9	0.9
492	0,9	0,9
518	0,722	0,9

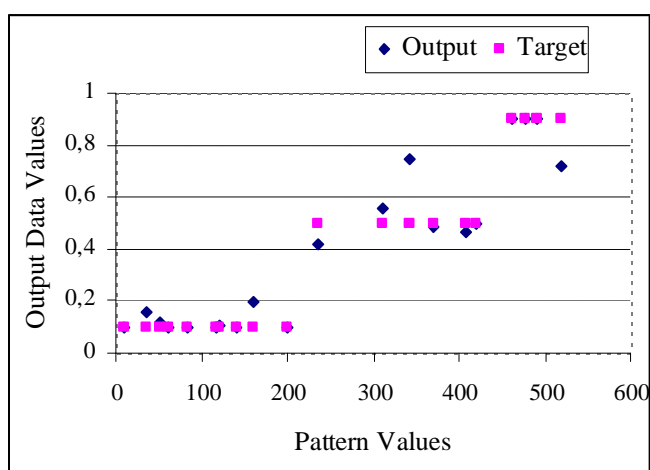


Fig. 13 Variation of the ANN Validation results together with the target data for Table 3.

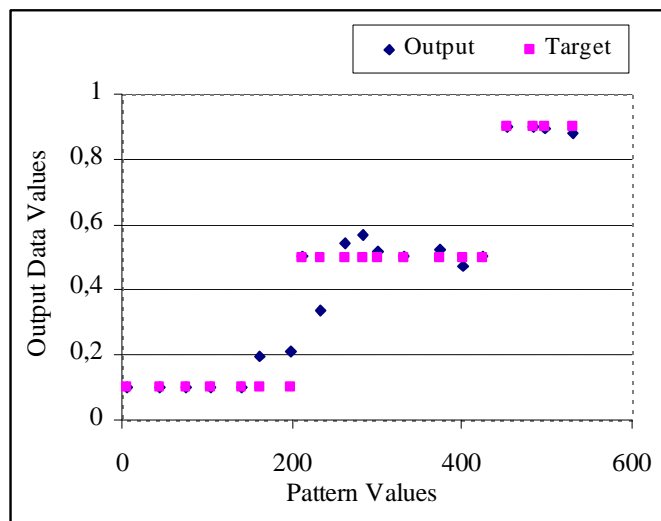


Fig. 14 Variation of the ANN Test results together with the target data for Table 4.

Table 4 Test results at various data points

Indices	Output	Target
6	0.1	0.1
45	0.1	0.1
75	0.1	0.1
105	0.1	0.1
141	0.1	0.1
163	0.1955	0.1
198	0.2088	0.1
213	0.5017	0.5
234	0.337	0.5
262	0.5412	0.5
284	0.5672	0.5
300	0,5162	0.5
331	0.501	0.5
374	0.5234	0.5
402	0.4713	0.5
425	0.5045	0.5
454	0.8998	0.9
485	0.8979	0.9
497	0.8951	0.9
530	0.8794	0.9

Improvement in Performance of Short Chorded Three – Phase Induction Motors With Variable PWM Switching Frequency, *Transaction on Magnetics, IEEE*, Vol. 42, No: 10, 2006, pp. 3452-3454.

[7] Y. Birbir, H. S. Nogay, Harmonic Variations in Three-phase Induction Motors Fed by PWM Inverter with Different Stator Coil Pitches, Proceedings of the 6th WSEAS Int. Conf. on Applications of Electrical Engineering, (AEE'07), Istanbul, Turkey, May, 27 -29, 2007

[8] Y. Birbir, H. S. Nogay, V. Topuz, Estimation of Total Harmonic Distortion in Short Chorded Induction Motors Using Artificial Neural Network, Proceedings of the 6th WSEAS Int. Conf. on Applications of Electrical Engineering, (AEE'07), Istanbul, Turkey, May 27 -29, 2007

[9] G. Chang, Modeling devices with nonlinear voltage-current characteristics for harmonic studies, *IEEE Trans. Power Del.* vol.19,no.4, pp.1802–1811, Oct. 2004.

[10] J. Nazarko, M. Poplawski, W. Zalewski, G. Cross, A. E. Walbridge, The Determination of Supply Harmonic Currents Produced by Multiple PWM Voltage Source Inverter Induction Motor Drives: An Expert System Approach, *Electric Power Engineering, PowerTech Budapest 99. International conference 29 Aug.-2 Sept. 1999* Page(s):93

[11] P. Gnacinski, Effect of unbalanced voltage on windings temperature, operational life and load carrying capacity of induction machine, *Energy Conversion and Management*, 49 (2008) 761–770.

[12] P. Gnacinski, Prediction of windings temperature rise in induction motors supplied with distorted voltage, *Energy Conversion and Management*, 49 (2008) 707–717

[13] R. Deshmukh, A. J. Moses, F. Anayi, Voltage harmonic variation in three-phase induction motors with different coil pitches, *Journal of Magnetism and Magnetic Materials* 304 (2006) e810–e812

[14] C. A. Hernandez-Aramburo, T. C. Green, S. Smith, Assessment of Power Losses of an Inverter-Driven Induction Machine With Its Experimental Validation, *IEEE Transaction on Industry Applications*, Vol. 39, NO. 4, July/August. 2003

[15] A. R. Muhoz and T. A. Lipo, Dual Stator Winding Induction Machine Drive, *IEEE Transactions on Industry Applications*, Vol. 36, No. 5, September/October 2000.

[16] D. H. Hwang, K. C. Lee, Y. J. Kim, Y. J. Lee, M. H. Kim, D. H. Kim, Analysis of Voltage Distribution in Stator Winding of IGBT PWM Inverter-Fed Induction Motors, *IEEE ISIE 2005*, June 20-23, Dubrovnik, Croatia, 2005.

[17] R. Ibtouen, S. Mekhtoub, O. Touhami, S. Bacha, A Novel Method for Modeling Magnetic

#### References:

[1] G. E. P. Box., G. Jenkins, Time Series Analysis, Forecasting and Control, *Golden-Day*, San Francisco, CA, 1970.

[2] M. S. Ballal, Z. J. Khan, ANN Based Stator Winding Inter-Turn Insulation Level Detector for Single Phase Induction Motor, *Technical Journals: Electrical Engineering, The Institution of Engineers (India)*, Vol : 86, Sep. 2005,

[3] T. M. Hagan., H. B. Demuth, M. Beale, Neural Network Design, *PWS Publishing Company*, 1996, 2-44.

[4] B. K. Bose., *Modern Power Electronics and Ac Drives*, Prentice Hall PTR, USA, 2002, pp. 625-689.

[5] C. Y. Lee, W.J. Lee, Y.N. Wang, J.C. Gu, Effect of Voltage Harmonics on the Electrical and Mechanical Performance of a Three-Phase Induction Motor, *Industrial and Commercial Power Systems Technical Conference*, Atlanta, Canada, 1998, IEEE 88-94.

[6] R. Deshmukh, A. J. Moses, F. Anayi,

Saturation in the Main Flux of Induction Machine, *Proceedings of the 5th WSEAS Int. Conf. on Systems Science and Simulation in Engineering*, Tenerife, Canary Islands, Spain, December 16-18, 2006

[18] H. S. Nogay, Y. Birbir, Designation of Harmonic Estimation ANN Model Using Experimental Data Obtained From Different Produced Induction Motors, *9<sup>th</sup> WSEAS Int. Conf. on Neural Networks (NN' 08)*, Sofia, Bulgaria, May., 2 - 4, (2008).

[19] Y. Birbir, H. S. Nogay, Y. Ozel, Estimation of Low Order Odd Current Harmonics in Short Chorded Induction Motors Using Artificial Neural Network, *9<sup>th</sup> WSEAS Int. Conf. on Neural Networks (NN' 08)*, Sofia, Bulgaria, May., 2 - 4, (2008).

[20] G. Bucci, E. Fiorucci, A. Ometto, N. Rotondale, On the Behavior of Induction Motors in Presence of Voltage Amplitude Modulations, *Proceedings of the 5th WSEAS Int. Conf. on Electric Power Systems High Voltage, Electric Machines*, Tenerife, Spain, December 16-18, 2005

[21] Temiz, C. Aküner, Y. Birbir, A. Kakilli, Rotating Field Voltage Analysis on the Stator and Rotor of the Inverted Rotor Induction Motor, *Proceedings of the 6th WSEAS Int. Conf. on Applications of Electrical Engineering, (AEE'07)*, Istanbul, Turkey, May 27 -29, 2007

[22] Y. Birbir, H. S. Nogay, S. Taskin, Prediction of Current Harmonics in Induction Motors with Artificial Neural Network, *International Aegean Conference on Electrical Machines and Power Electronics, IEEE, (ACEMP'07)*, Electromotion' 07 Joint Conference, Bodrum, Turkey, September, 10 – 12, 2007

[23] B. H. Ertan, M. Y. Uçtug, Modern Electrical Drives, *Springer - Verlag*, New York, USA, 2000

[24] H. A. Al-Rashidi, A. Gastli, A. Al-Badi, Optimisation of Variable Speed Induction Motor Efficiency Using Artificial Neural Networks, *Elsevier*, (2000).

[25] D. Mckinnon, D. Seyoum, C. Grantham, Rapid Determination of Fundamental and Harmonic RMS Quantities in a Three Phase System, *Elsevier*, The University of New South Wales, 2001.

[26] T. Wildi, Electrical Machines, Drives and Power Systems, *Sperika Enterprises Ltd.*, New Jersey, USA, 2002.

[27] J. J. Cathey, Electric Machines Analysis and Design Applying Matlab, *Mc Graw – Hill Companies*, Singapore, 2001.

[28] J. Arrillaga, B. C. Smith, N. R. Watson, A. R. Wood, Power System Harmonic Analysis, *John Wiley & Sons Ltd.*, England, 2000

[29] H. O. Mirzamani, A. L. Choobar, Study of harmonics effects on performance of induction motors, *8th WSEAS International Conference on CIRCUITS*, July 12, 2004, pp: 487-837.

[30] P. Pao-la-or, T. Kulworawanichpong, S. Sujitjorn, S. Peaiyoung, Computation of flux and electromagnetic force distributions in induction motors, *5th WSEAS / IASME International Conference on Electric Power Systems, High Voltages, Electric Machines (Power'05)*\_Friday, December 16, 2005, pp: 502-391

[31] G. Sharmila, P. Mahalingam, Harmonic Analysis of a Parallel Loaded Resonant Converter, *Proceedings of the 4th WSEAS International Conference on Power Engineering Systems (ICOPEs' 05)*, Rio de Janeiro, Brazil, April 25-27, 2005, Monday, April, 25, 2005

[32] Z. Wu and O. Ojo, Modeling of a Dual Stator Winding Induction Machine Including the Effect of Main Flux Linkage Magnetic Saturation, *1-4244-0365-0/06/\$20.00 (c),IEEE*, 2006